# Strong-Strong Beam-Beam Simulation Using a Green Function Approach

Ji Qiang, Miguel A. Furman, and Robert D. Ryne

MS 71J, Accelerator and Fusion Research Division
Lawrence Berkeley National Laboratory
Berkeley, CA 94720

**Abstract**

In this paper we present a new approach, based on a shifted Green function, to evaluate the electromagnetic field in a simulation of colliding beams. Unlike a conventional particle-mesh code, we use a method in which the computational mesh covers only the largest of the two colliding beams. This allows us to study long-range parasitic collisions accurately and efficiently. We have implemented this algorithm in a new parallel strong-strong beam-beam simulation code. As an application, we present a study of a beam sweeping scheme for the LBNL luminosity monitor of the Large Hadron Collider.

## 1 Introduction

The beam-beam interaction puts a strong limit on the performance of most colliders. At the interaction points, the electromagnetic fields generated by one beam focus or defocus the beam moving in the opposite direction. This can cause beam blowup and a reduction of luminosity. An accurate simulation of the beam-beam interaction will help to optimize the luminosity in high energy colliders. Macroparticle tracking provides an invaluable tool for the study of beam-beam interactions. In this approach, a number of simulation particles are generated with the same charge-to-mass ratio as the real particles. Outside the interaction region, each particle is transported using transfer maps associated with external elements, radiation damping, and quantum excitation. At interaction point, the electromagnetic fields from the colliding beams are calculated and applied to the opposite beam. To calculate the electromagnetic field requires the solution of the Poisson equation after each turn. The soft Gaussian approximation is usually used to obtain the electromagnetic fields quickly [1, 2, 3, 4, 5, 6, 7, 8]. To take into account the effects of the beam distribution self-consistently, one has to solve the Poisson equation numerically. Particle-mesh methods have been used to solve the Poisson equation on a numerical grid [9, 10, 11]. Using these methods, the computational cost for the Poisson solver can be on the order of $N_g^2 log(N_g)$, where $N_g$ is the number of grid points in one direction. Since these methods normally require using a mesh covering both beams, the straightforward application of such an approach would have strong disadvantages for two beams with large separation as in the long-range interaction [12]. Given that the electromagnetic fields in the empty space between the two beams are not needed, such an approach would be a waste of computational power, and would furthermore lead to poor numerical resolution on the grid for widely spaced beams. A hybrid fast multipole method has been proposed to calculate the electromagnetic field [12]. In this paper, we propose a particle-mesh method using a shifted Green function. Using such an approach, the computational domain

covers only the size of the largest beam. This avoids the potential loss of numerical resolution and leads to high computational efficiency since the fields between the bunches are not calculated.

The organization of this paper is as follows: The physical model and computational method are described in Section 2. Applications to the study of coherent beam-beam oscillations and beam sweeping in the Large Hadron Collider (LHC) are given in Section 3. The conclusions are drawn in Section 4.

## 2 Physical Model and Computational Method

In our beam-beam simulation, each charged particle has a position in phase space with coordinates $(x, x', y, y', \Delta z/\sigma_z, \Delta p_z/\sigma_{p_z})$. Here, a superscript prime denotes $\partial/\partial s$, where $s$ is the arc length. The motion of a particle will be subject to the influence of external fields, which provide transverse and longitudinal focusing of the beam. A particle will also lose energy through synchrotron radiation, i.e., through radiation damping and quantum excitation. The Coulomb interaction among charged particles within a bunch is negligible due to the cancellation of electric and magnetic forces at high energy. However, for the opposite-moving particles, the electric and magnetic forces will add up. This can significantly affect the motion of the particles in the other beam.

The effects of the external field can be represented, in the small-amplitude approximation, by a one-turn linear map. For our model, the map governing the horizontal motion is given by

$$\begin{pmatrix} x \\ x' \end{pmatrix}_{n+1} = \begin{pmatrix} \cos(2\pi\nu_{0x}) + \alpha_x \sin(2\pi\nu_{0x}) & \beta_x \sin(2\pi\nu_{0x}) \\ -\gamma_x \sin(2\pi\nu_{0x}) & \cos(2\pi\nu_{0x}) - \alpha_x \sin(2\pi\nu_{0x}) \end{pmatrix} \begin{pmatrix} x \\ x' \end{pmatrix}_n \tag{1}$$

where $\alpha_x$, $\beta_x$ and $\gamma_x$ are lattice functions at the interaction point, $\nu_{0x}$ is the horizontal lattice tune, and $n$ is the turn number. A similar map applies to the vertical phase space $y$ and $y'$ by replacing $x \to y$ in the above equation. For the longitudinal phase space, the one-turn map is defined by

$$\begin{pmatrix} \Delta z/\sigma_z \\ \Delta p_z/\sigma_{p_z} \end{pmatrix}_{n+1} = \begin{pmatrix} \cos(2\pi\nu_s) & \sin(2\pi\nu_s) \\ -\sin(2\pi\nu_s) & \cos(2\pi\nu_x) \end{pmatrix} \begin{pmatrix} \Delta z/\sigma_z \\ \Delta p_z/\sigma_{p_z} \end{pmatrix}_n \tag{2}$$

where $\nu_s$ is the synchrotron tune.

The effects of radiation damping and quantum excitation can be represented using a localized stochastic map. For each particle, the map consists of the following transformations [3]:

$$x_{n+1} = \lambda_x x_n + r_1 \sigma_x \sqrt{1-\lambda_x^2} \tag{3}$$

$$x'_{n+1} = \lambda_{x'} x'_n + r_2 \sigma_{x'} \sqrt{1-\lambda_{x'}^2} \tag{4}$$

$$y_{n+1} = \lambda_y y_n + r_3 \sigma_y \sqrt{1-\lambda_y^2} \tag{5}$$

$$y'_{n+1} = \lambda_{y'} y'_n + r_4 \sigma_{y'} \sqrt{1-\lambda_{y'}^2} \tag{6}$$

$$\Delta z_{n+1} = \lambda_z \Delta z_n + r_5 \sigma_z \sqrt{1-\lambda_z^2} \tag{7}$$

$$\Delta p_{z_{n+1}} = \lambda_{p_z} \Delta p_{z_n} + r_6 \sigma_{p_z} \sqrt{1-\lambda_{p_z}^2} \tag{8}$$

where the $\sigma$'s are the nominal rms equilibrium beam sizes in each dimension, the $\lambda$'s are given in terms of the damping time $\tau$ (measured in units of turns) by $\lambda_i = \exp(-1/\tau_i)$ where $i$ denotes $x$, $y$, or $z$, and the $r$'s are independent random numbers satisfying

$$\langle r_i \rangle = 0 \tag{9}$$
$$\langle r_i r_j \rangle = \delta_{ij} \tag{10}$$

The first term in the above transformation represents the radiation damping, and the second term represents the quantum excitation.

After applying the previous maps, the slopes of the particles are updated,

$$x'_{new} = x' + \Delta x' \tag{11}$$
$$y'_{new} = y' + \Delta y' \tag{12}$$

due to the beam-beam electromagnetic forces at the collision point. Here, the kick on a particle in beam 1 due to the influence of beam 2 is given by

$$\Delta x'_1 = \frac{2q_1 q_2 N_2}{\gamma_1 4\pi\epsilon_0 m_1 c^2} E_{x_2} \tag{13}$$
$$\Delta y'_1 = \frac{2q_1 q_2 N_2}{\gamma_1 4\pi\epsilon_0 m_1 c^2} E_{y_2} \tag{14}$$

where $\gamma$ is the relativistic factor, $\beta = |v|/c$, $c$ is the speed of light, $\epsilon_0$ is the vacuum permittivity, $q$ is the charge of a particle, $m$ is the rest mass of a particle, $N$ is the number of particles in a bunch, and $E_x$ and $E_y$ are the transverse electric fields generated by the opposing beam. The corresponding expression for the influence of beam 1 on particles in beam 2 is obtained by exchanging the subscripts 1 and 2.

For two relativistic colliding beams with large longitudinal-to-transverse aspect ratio, the electric field can be obtained from the solution of the two-dimensional Poisson equation. The general solution of Poisson's equation can be written as

$$\phi(x,y) = \int G(x,\bar{x},y,\bar{y})\rho(\bar{x},\bar{y})\, d\bar{x}d\bar{y} \tag{15}$$

where $G$ is Green's function and $\rho$ is the charge density. For the case of transverse open boundary conditions, Green's function is given by:

$$G(x,\bar{x},y,\bar{y}) = -\frac{1}{2}\ln((x-\bar{x})^2 + (y-\bar{y})^2) \tag{16}$$

Now consider a simulation of an open system where the computational domain containing the particles has a range of $(0, L_x)$ and $(0, L_y)$, and where each dimension has been discretized using $N_x$ and $N_y$ points. From Eq. 15, the electric potentials on the grid can be approximated as

$$\phi(x_i, y_j) = h_x h_y \sum_{i'=1}^{N_x} \sum_{j'=1}^{N_y} G(x_i - x_{i'}, y_i - y_{j'})\rho(x_{i'}, y_{j'}) \tag{17}$$

where $x_i = (i-1)h_x$ and $y_j = (j-1)h_y$. This convolution can be replaced by a cyclic convolution expression in a double-gridded computational domain [13, 14]:

$$\phi_c(x_i, y_j) = h_x h_y \sum_{i=1}^{2N_x} \sum_{j=1}^{2N_y} G_c(x_i - x_{i'}, y_i - y_{j'}) \rho_c(x_{i'}, y_{j'}) \tag{18}$$

where $i = 1, \cdots, 2N_x$, $j = 1, \cdots, 2N_y$, and

$$\rho_c(x_i, y_j) = \begin{cases} \rho(x_i, y_j) & : \ 1 \le i \le N_x; \ 1 \le j \le N_y \\ 0 & : \ N_x < i \le 2N_x \ or \ \ N_y < j \le 2N_y \end{cases} \tag{19}$$

$$G_c(x_i, y_j) = \begin{cases} G(x_i, y_j) & : \ 1 \le i \le N_x + 1; \ 1 \le j \le N_y + 1 \\ G(x_{2N_x - i + 2}, y_j) & : \ N_x + 1 < i \le 2N_x; \ 1 \le j \le N_y + 1 \\ G(x_i, y_{2N_y - j + 2}) & : \ 1 \le i \le N_x + 1; \ N_y + 1 < j \le 2N_y \\ G(x_{2N_x - i + 2}, y_{2N_y - j + 2}) & : \ N_x + 1 < i \le 2N_x; \ N_y + 1 < j \le 2N_y \end{cases} \tag{20}$$

$$\rho_c(x_i, y_j) = \rho_c(x_i + 2(L_x + h_x), y_j + 2(L_y + h_y)) \tag{21}$$

$$G_c(x_i, y_j) = G_c(x_i + 2(L_x + h_x), y_j + 2(L_y + h_y)) \tag{22}$$

From the above definition, one can show that the cyclic convolution will give the same electric potential as the convolution eq. 17 within the original domain, i.e.

$$\phi(x_i, y_j) = \phi_c(x_i, y_j) \qquad for \ \ i = 1, N_x; \ j = 1, N_y \tag{23}$$

The potential outside the original domain is incorrect but is irrelevant to the physical domain. Since both $G_c$ and $\rho_c$ are periodic functions, the convolution for $\phi_c$ in Eq. 18 can be computed efficiently using an FFT as described by Hockney et. al. [13].

In the above FFT-based algorithm, the particle domain and the electric field domain are contained in the same computational domain. Here, the particle domain is the configuration space containing the charged particles, and the field domain is the space where the electric field is generated by the charged particles in the particle domain. In the beam-beam interaction, two opposite moving beams might not overlap with each other. For example, in the long-range interaction, the two colliding beams could be separated more than $9\sigma$, where $\sigma$ is the rms size of the beam. The field domain where the electric field is generated by one beam can be different from the particle domain containing the beam. Fig. 1 shows a schematic plot of the two separated domains. In this figure, the particle domain has a range from $-R_0$ to $R_0$ for $x$ and $y$, and the field domain has a range from 0 to $2R_0$ for $x$ and $y$, where $R_0$ is maximum extent of the beam. To apply Hockney's algorithm directly will require the computational domain to contain both the particle domain and the field domain, i.e. both beams. Since there is a large empty space between two beams, containing both beams in one computational domain will result in a poor spatial resolution of the beams. This is also computationally inefficient because the electric fields in the empty space between two beams are not used. To avoid this problem, we have defined a shifted Green function as

$$G_s(x, \bar{x}, y, \bar{y}) = -\frac{1}{2} \ln((x_c + x - \bar{x})^2 + (y_c + y - \bar{y})^2) \tag{24}$$

where $x_c$ and $y_c$ are the center coordinates of the field domain. The electric potential in the field domain is written as

$$\phi(x + x_c, y + y_c) = \int G_s(x, \bar{x}, y, \bar{y}) \rho(\bar{x}, \bar{y}) \ d\bar{x} d\bar{y} \tag{25}$$

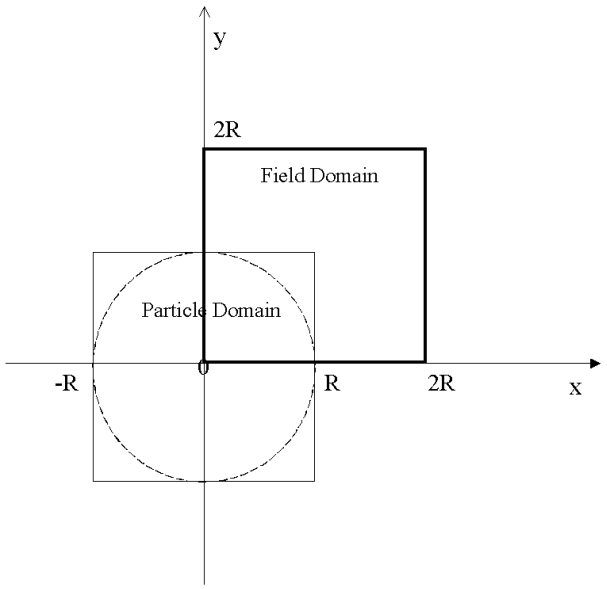


Figure 1: A schematic plot of the particle domain and the field domain.

Using the shifted Green function, the center of the field domain is shifted to the center of the particle domain. The range of $x$ and $y$ cover both the particle domain and the field domain in one computational domain. The FFT can be used to calculate the cyclic convolution in Eq. 18 using the new Green function. Here, on the doubled grids, the Green function is given as

$$G_c(x_i, y_j) = -\frac{1}{2} \begin{cases} \ln((x_c + x_i)^2 + (y_c + y_j)^2) & : \quad 1 \le i \le N_x;\ 1 \le j \le N_y \\ \ln((x_c - x_{2N_x - i + 2})^2 + (y_c + y_j)^2) & : \quad N_x < i \le 2N_x;\ 1 \le j \le N_y \\ \ln((x_c + x_i)^2 + (y_c - y_{2N_y - j + 2})^2) & : \quad 1 \le i \le N_x;\ N_y < i \le 2N_y \\ \ln((x_c - x_{2N_x - i + 2})^2 + (y_c - y_{2N_y - j + 2})^2) & : \quad N_x < i \le 2N_x;\ N_y < i \le 2N_y \end{cases} \tag{26}$$

Using the shifted Green function avoids the requirement that the particle domain and the field domain be contained in one big computational domain. This leads to good numerical resolution for the charge densities and resulting electric fields, because the empty space between the beams is not included in the calculation. This is also far more efficient, in terms of computational effort and storage, than the traditional approach of gridding the entire problem domain.

As an example of the above FFT-based algorithms, we computed the radial electric field distribution generated by a round beam with a Gaussian density distribution using the particle domain and the field domain shown in Fig. 1. Fig. 2 shows the radial electric field $E_r$ as a function of distance along the diagonal line of the particle domain using the conventional algorithm, i.e. without the shifted Green function, and 128x128 grid. The electric field from the analytical calculation is also given in the same figure for comparison. It is seen that the agreement between the numerical solution and the analytical calculation is excellent. As a test of the shifted Green function approach, we also computed the electric field $E_r$ along the diagonal line of the field domain. The results are shown in Fig. 3 together with the the analytical calculation. We see that

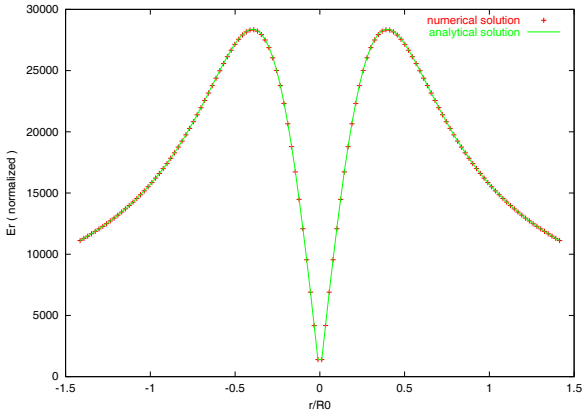


Figure 2: Radial electric field as a function of distance along the diagonal line of the particle domain.

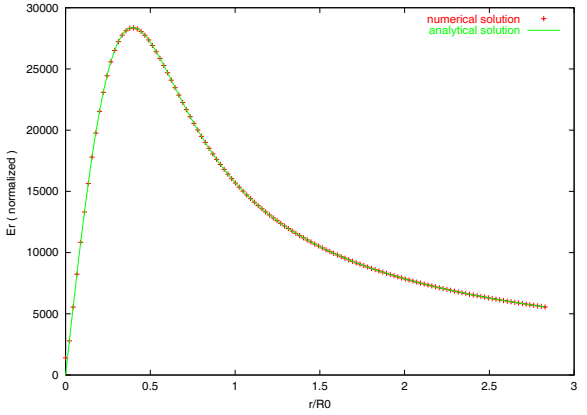


Figure 3: Radial electric field as a function of distance along the diagonal line of the field domain.

Table 1: LHC nominal beam-beam parameters

| | |
|---|---|
| beam energy (TeV) | 7 |
| protons per bunch | $1.05 \times 10^{11}$ |
| $\beta^*$ (m) | 0.5 |
| RMS spot size at the IP ($\mu m$) | 15.9 |
| betatron tunes ($\nu_x$, $\nu_y$) | (0.31, 0.32) |
| RMS bunch length (m) | 0.077 |
| synchrotron tune $\nu_z$ | 0.0021 |

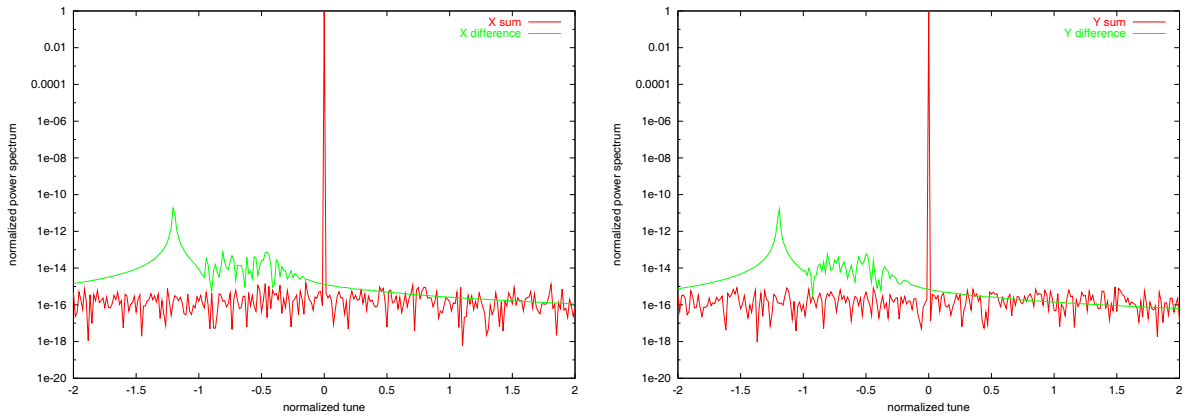


Figure 4: Spectra of the horizontal (left) and vertical (right) sum and the difference centroid motion for nominal beam-beam collision parameters.

the two solutions are in excellent agreement.

## 3 Applications

As a first application, we have studied the coherent beam-beam dipole oscillation in the proposed Large Hadron Collider (LHC). The nominal beam-beam parameters of LHC are given in Table 1.

In this study, the two proton beams are assumed to have the same physical parameters. The nominal beam-beam parameter $\xi$ is $-0.0034$. Here $\xi$ is defined as $-\frac{r_p N \beta_x}{4\pi\gamma\sigma_x^2}$ and $r_p$ is the classical proton radius. Fig. 4 shows the spectra of the sum and the difference of the beam centroids for the nominal LHC parameters. The normalized tune is defined as $(\nu - \nu_{x0})/|\xi|$, where $\nu_{x0}$ is the horizontal bare tune, and where $\nu$ is the power spectrum associated with the sum or the difference of the centroid motion of the two beams. The simulation was run for 20000 turns using a single slice model for each beam with one million particles and a $128 \times 128$ grid. The centroid of one beam is initially displaced by $0.01\sigma$ on the horizontal plane and the vertical plane. Only head-on collisions were taken into account in this simulation. It is seen that there exist two oscillation frequencies for the centroid motion, one corresponding to the bare tune without beam-beam interaction (the $\sigma$ mode) and the other (the $\pi$ mode) with its frequency shifted downwards in tune by $(1.21 \pm 0.015)|\xi|$ in $x$ and by $(1.19 \pm 0.015)|\xi|$ in $y$, where the uncertainty 0.015 is due to the finite number of turns used in the simulation. The frequency downshift has also been

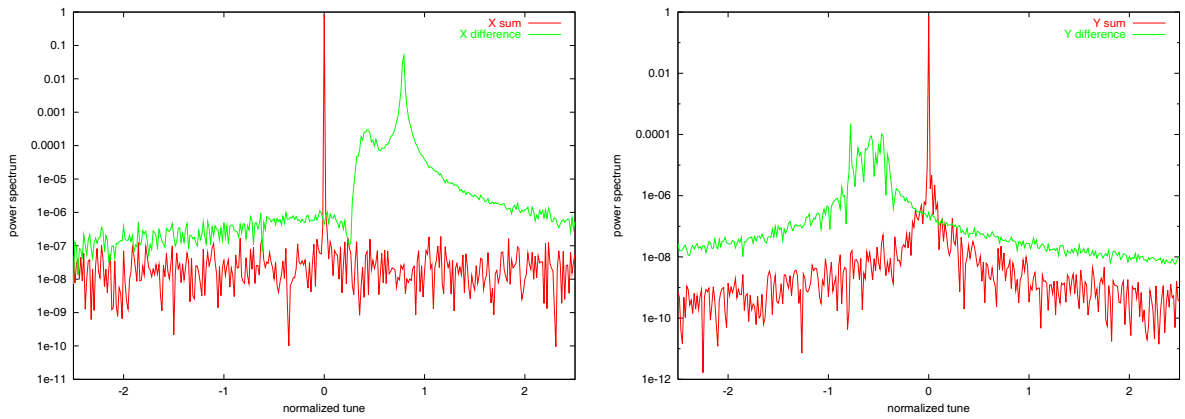


Figure 5: Spectra of the horizontal (left) and vertical sum and difference centroid motion for long-range beam-beam collision with $9\sigma_x$ horizontal separation.

calculated using a linearized Vlasov analysis which gives $1.21\xi$ [15]. We see that the simulation result agrees with the theoretical calculation within 2%.

The same model was also employed to simulate the long-range parasitic collisions in the LHC. To reduce the computing time, we lumped all parasitic collisions into a single collision. A static dipole kick from the long-range collision was subtracted following the treatment of Herr et. al. [12]. The beam-beam kick in the long range interaction is given by:

$$\Delta x'_{2,1} = n_{par}\frac{2q_1q_2N_{1,2}}{\gamma_{2,1}4\pi\epsilon_0 m_{2,1}c^2}(E_{x_{1,2}} - D\frac{1}{L_x\sigma_x}(1.0 - \exp(-\frac{L_x^2}{2}))) \quad (27)$$

$$\Delta y'_{2,1} = n_{par}\frac{2q_1q_2N_{1,2}}{\gamma_{2,1}4\pi\epsilon_0 m_{2,1}c^2}(E_{y_{1,2}} - D\frac{1}{L_y\sigma_y}(1.0 - \exp(-\frac{L_y^2}{2}))) \quad (28)$$

where $L_x\sigma_x$ is the horizontal separation distance of the two beams, $L_y\sigma_y$ is the vertical separation distance, $D$ is a sign function depending on the relative position of the two beams, and $n_{par}$ is the number of parasitic collisions. In the above equations, the static dipole kick is approximated by a constant dipole kick generated by a Gaussian distribution at a distance $x = L_x\sigma_x$ or $y = L_y\sigma_y$. Fig. 5 shows the spectra of the sum and the difference of the beam centroids with $9\sigma_x$ horizontal separation. Here, only long-range interactions are included with 16 parasitic collisions. In the horizontal plane, the $\pi$ mode frequency is shifted upward instead of downward as opposed to the no-separation collision case in Fig. 4. The normalized tune shifts of the $\pi$ mode are $(0.79 \pm 0.015, -0.78 \pm 0.015)$. The numerical parameters are the same as those used in the nominal LHC simulation without separation. Since the transverse distance between the two beams at the parasitic collision points is significantly larger than the rms size of the beams, the effects of the beam distribution on the coherent motion might not be important. The beams might be treated as rigid bunches. In this case, the contribution of the long range beam-beam interaction to the tune shift of the coherent oscillation modes would be twice the incoherent long-range tune shift, which is proportion to $1/L_x^2$. Fig. 6 shows the values of the $\pi$ mode tune shifts at several different horizontal separations, along with a curve having the $1/L_x^2$ dependence. We see that the tune shifts fit the $1/L_x^2$ scale very well.

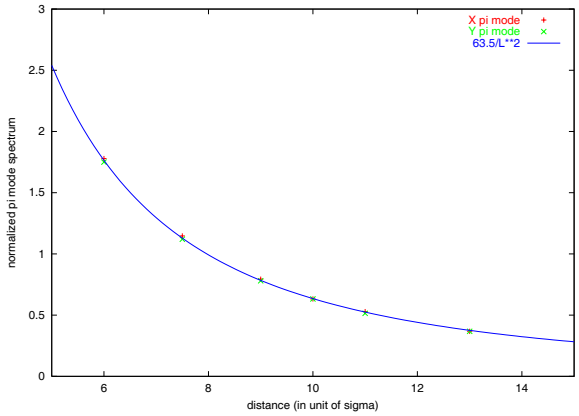


Figure 6: Normalized $\pi$ mode tune shift as a function of horizontal separation for the case of long-range beam-beam collisions.

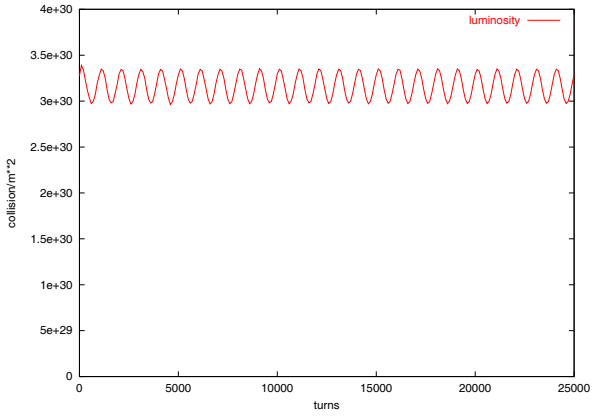


Figure 7: The luminosity per collision as a function of turns during the sweeping process.

In the luminosity monitoring scheme being developed at LBNL for the LHC, one beam is deliberately swept in a circle about the geometrical collision point, where the other beam remains fixed [16, 17]. This sweeping can be achieved by an appropriate time-dependent closed orbit bump spanning the interaction point. As a test, we have chosen a sweeping period of 1000 turns and a sweeping radius of $0.6\sigma_0$ for the closed orbit of beam 2, while the closed orbit of beam 1 remains static and is offset by $0.2\sigma_0$ from the nominal interaction point at 45 degrees relative to the horizontal axis. Fig. 7 shows the luminosity per collision as a function of turns during the process of sweeping. It is seen that the luminosity oscillates due to the off-center collisions with a period of 1000 turns. In practice, this is the signal that could be used to optimize the luminosity. Fig. 8 shows the normalized rms emittances as a function of turns during the sweeping process. There is no significant emittance growth after 55000 turns except for a slightly initial increase that can be attributed to particle redistribution. However, we have found that, when the number of charged particles per bunch is increased by a factor of 10, $3-4\%$ emittance growth is observed after 55000 turns. Fig. 9 shows the beam centroid spectra of two sweeping beams. Comparing with the nominal case in Fig. 4, we see that the tune shifts of the $\pi$ modes are smaller during the

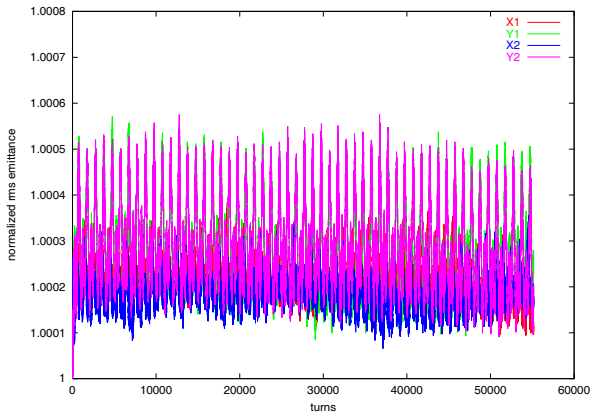


Figure 8: The rms emittance as a function of turns during the sweeping process.

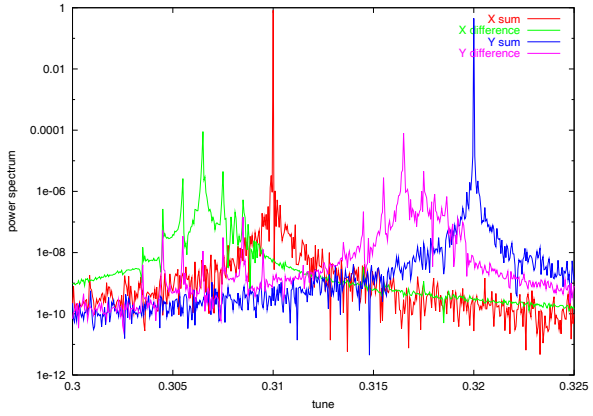


Figure 9: Spectra of the sum and difference centroid motion during the sweeping process.

sweeping operation owing to the lower effective beam-beam parameter. The difference spectra also show sidebands of the $\pi$ modes separated by 0.001, corresponding to the sweeping tune.

## 4 Conclusions

In this paper, we have presented an FFT-based method to evaluate the electromagnetic field in the study of the strong-strong beam-beam interaction. Using such a method, we can handle not only the on-axis head-on beam-beam collision but also the long-range beam-beam collision with arbitrary separation without losing computational efficiency. A study of the coherent tune shift for the beam-beam interaction shows good agreement with the theoretical prediction. As an application, we have also studied a luminosity monitoring scheme for LHC based on beam sweeping. In our simulations, there is no significant beam quality degradation after 55000 turns for the nominal parameter values.

## Acknowledgments

This work was performed on the Cray T3E and IBM SP at the National Energy Research Scientific Computing Center located at Lawrence Berkeley National Laboratory. This work was supported by the U.S. Department of Energy, Office of Science, Division of High Energy and Nuclear Physics, under the project, Advanced Computing for 21st Century Accelerator Science and Technology.

## References

[1] K. Hirata, H. Moshammer and F. Ruggiero, Particle Accelerators **40**, 205 (1993).

[2] K. Hirata, Phys. Rev. Lett. **20**, 2228 (1995).

[3] M. A. Furman, A. Zholents, T. Chen, and D. Shatilov, "Comparisons of Beam-Beam Code Simulations," CBP Tech Note-59, 1996.

[4] Y. Papaphilippou and F. Zimmermann, PRST-AB **2**, 104001 (1999).

[5] M. A. Furman, "Beam-Beam Simulations with the Gaussian Code TRS", LBNL-42669, CBP Note 272 (1999).

[6] T. Koyama, PRST-AB **2**, 024001 (1999).

[7] L. H. A. Leunissen, F. Schmidt, G. Ripken, PRST-AB **3**, 124002 (2000).

[8] M. P. Zorzano and F. Zimmermann, PRST-AB **3**, 044401 (2000).

[9] S. Krishnagopal and R. Siemann, Phys. Rev. Lett. **28**, 2461 (1991).

[10] E. B. Anderson, T. I. Banks, J. T. Rogers, "ODYSSEUS: Description of and Results from a Strong-Strong Beam-Beam Simulation for Storage Rings," p. 1686, Proceedings of the 1999 Particle Accelerator Conference, New York, 1999.

[11] Y. Cai, A. W. Chao, S. I. Tzenov, and T. Tajima, PRST-AB **4**, 011001 (2001).

[12] W. Herr, M. P. Zorzano, F. Jones, PRST-AB **4**, 054402 (2001).

[13] R. W. Hockney and J. E. Eastwood, "Computer Simulation Using Particles," McGraw-Hill Book Company, New York, 1985.

[14] J. W. Eastwood and D. R. K. Brownrigg, J. Comp. Phys. **32**, 24 (1979).

[15] K. Yokoya and H. Koiso, Part. Accel. **27**, 181 (1990).

[16] S. Krishnagopal and M. A. Furman and W. C. Turner, "Studies of the Beam-Beam Interaction for the LHC," LBNL-43061, CBP Note 308 (1999).

[17] M. A. Furman and W. C. Turner, "Beam-Beam Simulations for Separated Beams in the LHC", LBNL-46223, CBP Note 350 (2000).